Progress in Oceanography 223 (2024) 103232

Contents lists available at ScienceDirect

Progress in Oceanography

journal homepage: www.elsevier.com/locate/pocean

Offshore high chlorophyll eddies: Separating upwelling from nearshore migration from ocean color remote sensing

Qing Zhu [*], Zhongping Lee

State Key Laboratory of Marine Environmental Science, College of Ocean and Earth Sciences, Xiamen University, Xiamen 361102, China

ARTICLE INFO

Keywords:
Offshore eddies
Sources of blooming phytoplankton
Gaussian absorption peaks
Two-dimensional spatial model
California offshore region

ABSTRACT

Offshore eddies are often associated with high amounts of phytoplankton (represented by the chlorophyll-a concentration (Chla)), or, phytoplankton blooms, which can be detected from ocean color satellites. The phytoplankton “blooms” in these eddies are commonly explained as a result of enhanced nutrients - local growth - brought up from deeper waters by these eddies, although potentially they could simply be a migration of high Chla waters from nearshore regions. To better understand the interactions between physical forcing and phytoplankton dynamics, it is necessary to separate these “blooms” between local growth and migration. In this study, we first updated the multiple pigment inversion model using a synthetic dataset, for retrieving the absorption coefficient and absorption Gaussian peaks of phytoplankton from remote sensing reflectance in the broad aquatic environments. On this basis, a two-dimensional spatial model was developed to identify the sources of phytoplankton associated with offshore eddies. The model was based on the absorption coefficient of phytoplankton at 443 nm ($a_{ph}(443)$) and the ratio of two Gaussian peaks at 519 nm and 435 nm, where these two peaks represent different contributions of phytoplankton pigments to a_{ph}. This two-dimensional spatial model was applied to images collected by the Ocean and Land Color Instrument in the California offshore region to demonstrate that the scheme effectively separated offshore upwelling waters from those migrating from nearshore waters. Such separations provide independent sources for identifying offshore upwelling water that will be important for studying offshore circulation processes.

1. Introduction

Ocean eddies are fundamental dynamic processes in oceans. They are essential for ocean mass transport (Zhang et al., 2014), play important roles in particulate organic carbon distribution (Amos et al., 2019), silica export (Benitez-Nelson et al., 2007), transports of heat and salt fluxes (Amores et al., 2017; Dong et al., 2014; Hausmann and Czaja, 2012), changes in bio-optical properties (Siegel et al., 2008, 2011) and phytoplankton community structure (Laiolo et al., 2016; Romero et al., 2016). Sea surface height (SSH) fields observed using satellite altimeters are commonly used for eddy detection (Chelton et al., 2007, 2011b). Eddies also tend to affect phytoplankton distribution (Chelton et al., 2011a; Frenger et al., 2018; Gaube et al., 2014; He et al., 2021), where high amounts of phytoplankton (represented by chlorophyll-a concentration (Chla)) waters associated with eddies are commonly observed by ocean color satellites (Chen et al., 2022; Hong et al., 2023). For example, Chen et al. (2022) observed an eddy-like bloom on August 28th, 2007, in the western South China Sea using the Moderate Resolution Imaging Spectroradiometer derived Chla data; Hong et al. (2023) observed the phytoplankton bloom associated with eddy on May 8th, 2011, in the East/Japan Sea using the Geostationary Ocean Color Imager derived Chla data.

One common explanation for the presence of these eddy-related phytoplankton bloom waters is that adequate nutrients are brought up through vertical pumping by such eddies, which supports the growth of phytoplankton (Chen and Tang, 2012; Tang et al., 2002), commonly termed as eddy pumping or eddy-Ekman pumping (Falkowski et al., 1991; Gaube et al., 2013; Klein and Lapeyre, 2009; McGillicuddy et al., 1998, 2007). Another possible reason for such high Chla offshore waters is the horizontal migration of high-Chla or high-nutrient waters from nearby coastal waters by eddy-related circulation dynamics (Chen et al., 2022; Lin et al., 2010; Rubio et al., 2018), such as eddy trapping and subsequent horizontal transport (Gaube et al., 2014; Lehahn et al., 2011). As there are usually two different processes (upwelling vs. no-upwelling) for such eddies, for better understanding of offshore dynamics, it is necessary to separate these processes, where a single SSH

---

[*] Corresponding author.
E-mail addresses: qz@xmu.edu.cn (Q. Zhu), zhongping.lee@umb.edu (Z. Lee).

https://doi.org/10.1016/j.pocean.2024.103232
Received 3 October 2023; Received in revised form 3 February 2024; Accepted 26 February 2024
Available online 27 February 2024
0079-6611/© 2024 Elsevier Ltd. All rights reserved.

Table 1
Minimum, maximum, average, and standard deviation values of $a_{ph}(440)$, $a_g(440)$, $a_{dm}(440)$, $b_{bph}(440)$, $b_{bdm}(440)$, and $R_{rs}(440)$ in our used synthetic dataset.

IOPs and R_{rs}	Minimum value	Maximum value	Average Value	Standard deviation
$a_{ph}(440)$ (m^{-1})	0.00138	0.97	0.064	0.107
$a_g(440)$ (m^{-1})	0.00022	1.15	0.151	0.208
$a_{dm}(440)$ (m^{-1})	0.00036	0.80	0.042	0.082
$b_{bph}(440)$ (m^{-1})	0.00003	0.06	0.003	0.005
$b_{bdm}(440)$ (m^{-1})	0.00087	0.01	0.004	0.003
$R_{rs}(440)$ (sr^{-1})	0.00020	0.02	0.005	0.005

image is short of information for the separation.

The California Current System (CCS) is characterized with frequent eddies (Chaigneau et al., 2009; Kurian et al., 2011), making it an ideal area for studying the origin of “blooming” phytoplankton in offshore eddies, thus separating upwelling eddies from those due to the transportation of nearshore waters. Previous studies have found that eddies can transport coastal waters to the offshore in the CCS (Chenillat et al., 2015; Krause et al., 2020; Nagai et al., 2015); thus, these phytoplankton blooms may be drifters. In contrast, He et al. (2017) found that phytoplankton blooms were locally generated in an anticyclonic eddy owing to eddy-Ekman pumping and winter mixing in the nutrient-depleted southeastern Indian Ocean. Similar scenarios may also occur in the CCS, as eddy-Ekman pumping is also frequent in this region (Pickett and Paduan, 2003; Seo et al., 2016); thus, these phytoplankton may also originate from local growth. However, to the best of our knowledge, there have been no studies trying to separate these two types of processes from ocean color remote sensing.

Through sampling of an eddy propagated westward in the northern Gulf of Alaska during May and September of 2003, Ladd et al. (2005) found that the water properties in the eddy core were similar to the historical water near Yakutat and distinct from the surrounding water. Therefore, when the eddy moves to the offshore, the physical and chemical properties of the source water in the eddy center could remain stable. In addition, Moore et al. (2007) and Batten and Crawford (2005) reported that eddies can export coastal phytoplankton communities offshore. Huang et al. (2010) also illustrated that coastal phytoplankton species could live well in the coast-formed eddies when they moved to the offshore. For migrators, as the phytoplankton share the same origin as those of nearshore high Chla waters, thus, they have similar phytoplankton community structures. However, for blooming phytoplankton from local growth, owing to different nutrient sources and physical properties of water, their community structure will be different from that of phytoplankton in the nearshore waters (Huang et al., 2010; Moore et al., 2007). Furthermore, different phytoplankton communities have different pigment compositions, and different pigments have different absorption signals (Bidigare et al., 1990; Bricaud et al., 2004), they provide us a basis for separating these two origins in blooming phytoplankton eddies from ocean color satellite remote sensing, where the phytoplankton absorption coefficient (a_{ph}, which represents the total absorption signals of different pigments) can be derived from ocean color measurements. In turn, this identification of origin further helps to separate offshore eddies into vertical mixing and migration of coastal waters.

The a_{ph} spectrum is a sum of contributions from different pigments (Bricaud et al., 2004; Hoepffner and Sathyendranath, 1991), where different pigment compositions suggest different phytoplankton communities (Jeffrey et al., 2011), thus a decomposition of a_{ph} spectrum can be used to reveal phytoplankton communities or phytoplankton functional groups (PFGs) information (Sun et al., 2022; Wang et al., 2016, 2017, 2018; Zhang et al., 2018). In this study, we updated the multiple pigment inversion (MuPI) model developed by Wang et al. (2016) for the decomposition of a_{ph} spectrum from remote sensing reflectance (R_{rs}) under different water environments. From the retrieved $a_{ph}(443)$ and two Gaussian peaks contributing to a_{ph}, we constructed a two-dimensional spatial model to separate the origin of blooming phytoplankton associated with offshore eddy waters. We further applied this scheme to the Ocean and Land Color Instrument (OLCI) measurements in the California offshore region and other areas to identify the origin of eddies associated with high Chla. This scheme and its results extend the value of ocean color remote sensing for studying circulation dynamics in offshore regions.

This paper is organized as follows. In Section 2, we present the dataset used in this study. In Section 3, we mainly describe the Gaussian peaks retrieval and the separation scheme construction. In Section 4, accuracy evaluation results of Gaussian peaks retrieval and two application cases are presented. In Section 5, we further evaluate the identification accuracy of the scheme on multiple images in the California offshore region, and also discuss the applicability of our scheme to other offshore waters. In Section 6, we summarize the scheme construction and main findings in this study.

2. Dataset

2.1. Synthetic dataset

As we want to apply the separation scheme to different water environments in different sea areas, we adopted a synthetic dataset under broad aquatic environment (Lee et al., 2018, 2019), with a wavelength range of 350–700 nm and a spectral resolution of 5 nm, to update the MuPI model. In this dataset, a_{ph} were selected from $>$ 4,000 a_{ph} spectra in the National Aeronautics and Space Administration (NASA) SeaWiFS Bio-optical Archive and Storage System (SeaBASS) dataset (https://seabass.gsfc.nasa.gov) and from our own collections (Wang et al., 2021). The absorption coefficient of pure seawater (a_w) in the range of 350–550 nm were from Lee et al. (2015), and their values in the range of 555–700 nm were from Pope and Fry (1997). The values of the backscattering coefficient of pure seawater (b_{bw}) were from the literature Zhang et al. (2009). For other inherent optical properties (IOPs), such as the absorption coefficient of colored dissolved organic matter (a_g), absorption coefficient of non-pigmented particulate matter (a_{dm}), backscattering coefficient of phytoplankton (b_{bph}), and backscattering coefficient of non-pigmented particulate matter (b_{bdm}), were simulated using relevant parameterized models, as described in detail in IOCCG Report 5 (IOCCG, 2006; IOCCG-OCAG, 2003). Based on these IOPs, R_{rs} data were finally simulated using HydroLight (Mobley and Sundman, 2013). The dataset contained 720 sets of data, covering oligotrophic to eutrophic waters, and eventually 571 sets of data were used in this study after excluding a few duplicates and special cases ($a_{ph}(440) > 1.0\ m^{-1}$). Seventy percent (400 sets) of this dataset were used to update the model parameters (the linear relationship between different phytoplankton absorption Gaussian peaks, average Gaussian peak center wavelengths and widths), with the remaining thirty percent (171 sets) used for model validation. Table 1 provides the statistical distribution of the synthetic dataset we used, taking 440 nm as an example.

2.2. Satellite ocean color data

OLCI data (R_{rs} and Chla) over the California offshore region, downloaded from the NASA Goddard Space Flight Center (https://oceancolor.gsfc.nasa.gov), were used to demonstrate the scheme to separate the origin of blooming phytoplankton in offshore eddies. Daily Level 2 R_{rs} products with a spatial resolution of 300 m were used to retrieve phytoplankton absorption Gaussian peaks. Specifically, as examples, Level 2 R_{rs} data acquired on June 4th, 2017, and July 5th, 2020, were selected to demonstrate the scheme on separating the origin of blooming phytoplankton in the California offshore eddies (see Section 4.2 and

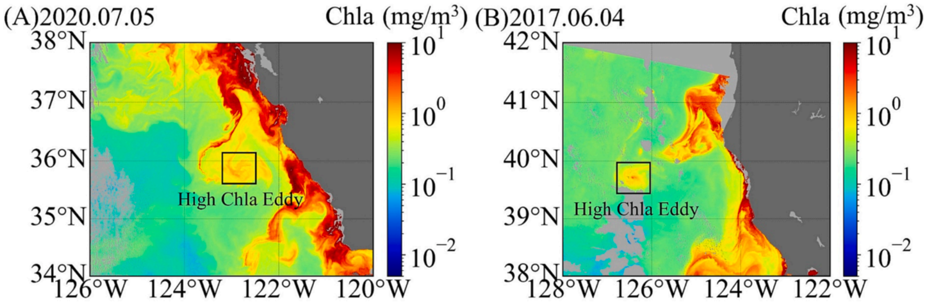

Fig. 1. Chlorophyll-a concentration in the California offshore waters observed using the Ocean and Land Color Instrument on (A) July 5th, 2020, and (B) June 4th, 2017. The high chlorophyll-a concentration waters associated with eddies were framed with black rectangles and marked nearby.

Section 4.3). Fig. 1 shows the blooming phytoplankton associated with these eddies in the California offshore waters of these two days (framed with black rectangles and marked nearby). Furthermore, our scheme was applied to multiple images acquired during the spring and summer (March to August) of 2017 in the California offshore, specifically on the dates of 2017.05.11, 2017.05.12, 2017.06.08, 2017.06.11, 2017.07.08, and 2017.07.21, to assess its determination accuracy (see Section 5.1). We also applied our scheme to other images of offshore waters, including the offshore waters in the Canary Current System, the Peru–Chile Current System, the Benguela Current System, and the South China Sea and adjacent Taiwan Strait, on various dates to evaluate the scheme (see Section 5.2).

2.3. *Sea level anomaly data*

As an independent data source for tracking the movement trajectories of eddies, the daily sea level anomaly (SLA) data obtained from satellite altimeters (0.25°×0.25° resolution, product identifier: SEALEVEL_GLO_PHY_L4_MY_008_047) in the California offshore region and four other application areas were downloaded from the Copernicus Marine Environment Monitoring Service (CMEMS) website (https://data.marine.copernicus.eu/products). The SLA data were computed with respect to the 20-year mean (1993–2012) and estimated by optimal interpolation. We used SLA data from May 23rd to July 5th, 2020, to validate our separation results in the California offshore region on July 5th, 2020 (see Section 4.2); additionally, we used the SLA data from May 25th to June 4th, 2017, to identify the upwelling-associated eddy in the California offshore region on June 4th, 2017 (see Section 4.3). Furthermore, SLA data collected during the spring and summer of 2017 in the California offshore region were used to track the origin of blooming phytoplankton in the offshore eddies during this period (see Section 5.1). Daily SLA data were also used to track eddies in the offshore waters in the Canary Current System (August 24th to September 2nd, 2017), the Peru–Chile Current System (April 25th to May 10th, 2017), the Benguela Current System (November 12th to November 25th, 2017), and the South China Sea and adjacent Taiwan Strait (July 2nd to July 16th, 2017) (see Section 5.2).

3. Method

3.1. *Retrieval of phytoplankton absorption Gaussian peaks*

Wang et al. (2016, 2017) proposed the MuPI model for retrieving phytoplankton absorption Gaussian peaks from R_{rs} in inland cyanobacteria bloom waters. The model includes Gaussian decomposition of a_{ph} and further spectral optimization for retrieving Gaussian peaks from R_{rs}. In the model, R_{rs} is the input, the Gaussian peaks and other IOPs (i.e., $a_{dg}(\lambda)$, the total absorption coefficient of non-pigmented particulate matter and colored dissolved organic matter; $b_{bp}(\lambda)$, the backscattering coefficient of particulate matter) are the outputs. To apply this approach to a broader aquatic environment, we updated the MuPI model parameters using a synthetic dataset (see Section 2.1). In this study, there are two steps for retrieving Gaussian peaks from R_{rs}, including update of Gaussian parameters from a_{ph} (i.e., the linear relationship between different Gaussian peaks, average Gaussian peak center wavelengths and widths), and further Gaussian peaks retrieval from R_{rs}.

Following Hoepffner and Sathyendranath (1991), an a_{ph} spectrum can be modeled through the sum of several Gaussian curves, and each Gaussian curve represents the contribution to the absorption coefficient by a specific pigment (chlorophyll, carotenoid, phycoerythrin, etc.). The Gaussian decomposition is described with Eq. (1), where $a_{ph}(\lambda)$ represents the absorption coefficient of phytoplankton, $a\text{Gau}(\lambda_i)$, λ_i, and σ_i represent phytoplankton absorption Gaussian peak, Gaussian peak center wavelength, and width of the ith Gaussian curve, respectively. In this study, there are a total of 13 Gaussian curves that correspond to the absorption coefficients of different pigments.

$$a_{ph}(\lambda) = \sum_{i=1}^{n} a\text{Gau}(\lambda_i) \times \exp\left[-0.5\left(\frac{\lambda-\lambda_i}{\sigma_i}\right)^2\right] \tag{1}$$

Fig. 2 (A) presents the overall flowchart of Gaussian parameters update from a_{ph}, based on 13 initial values of $a\text{Gau}(\lambda)$s, Gaussian peak center wavelengths, and widths, respectively, a_{ph} were then modeled following Eq. (1). Specifically, the initial Gaussian peak center wavelengths were determined using the first and second derivatives of a_{ph} were zeros, and also referred to relevant literature (Bricaud et al., 2004; Hoepffner and Sathyendranath, 1991; Wang et al., 2016); the initial widths were determined with reference to Chase et al. (2013) and Wang et al. (2016). The spectral proximities between the measured and modeled a_{ph} spectra were quantified by a target function, which was the same as that used by Wang et al. (2016). Minimizing the target function through continuous iteration, the $a\text{Gau}(\lambda)$s, Gaussian peak center wavelengths, and widths of each a_{ph} spectrum can be calculated, and the average outputs of these parameters are shown in Table S1 in the supplementary material. To simplify the calculation for $a\text{Gau}(\lambda)$s retrieval from R_{rs}, 13 $a\text{Gau}(\lambda)$s were simplified to $a\text{Gau}(435)$ and $a\text{Gau}(519)$ through linear transformation, and the linear relationship between these two $a\text{Gau}(\lambda)$s and other $a\text{Gau}(\lambda)$s are also presented in Table S1 in the supplementary material. As a result, each a_{ph} spectrum can be modeled from $a\text{Gau}(435)$ and $a\text{Gau}(519)$ after Gaussian parameters update.

The functional relationship between R_{rs} and IOPs can be expressed using Eqs. (2)–(4) (Gordon et al., 1988; Lee et al., 2002).

$$R_{rs}(\lambda) = \frac{0.52^{*} r_{rs}(\lambda)}{1 - 1.7^{*} r_{rs}(\lambda)} \tag{2}$$

$$r_{rs}(\lambda) = 0.089^{*}\text{u}(\lambda) + 0.125^{*}\text{u}(\lambda)^2 \tag{3}$$

$$\text{u}(\lambda) = b_b(\lambda)/(a_t(\lambda) + b_b(\lambda)) \tag{4}$$

With $r_{rs}(\lambda)$ for the below-surface remote sensing reflectance; $b_b(\lambda)$ for the total backscattering coefficient; and $a_t(\lambda)$ for the total absorption coefficient of a water body. $b_b(\lambda)$ and $a_t(\lambda)$ can be described as the sum of

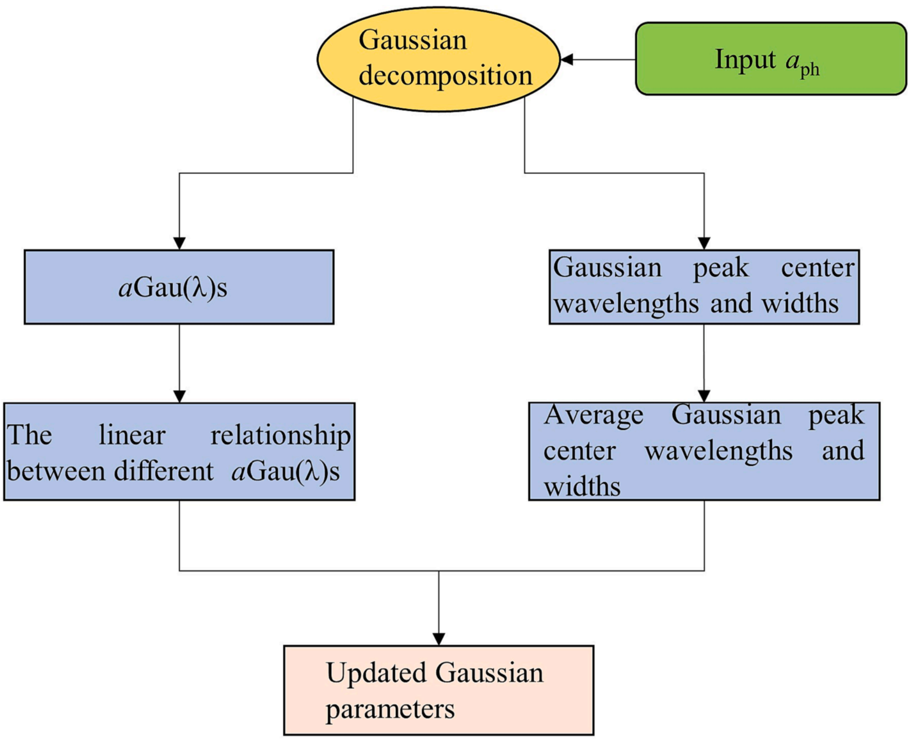

Fig. 2a. Flowchart of Gaussian parameters update from a_{ph}.

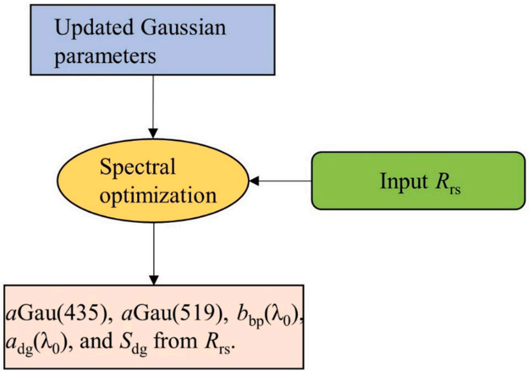

Fig. 2b. Flowchart of phytoplankton absorption Gaussian peaks (aGau(λ)s) retrieval from R_{rs}.

relevant components using Eqs. (5)–(6) (Prieur and Sathyendranath, 1981; Roesler et al., 1989; Sathyendranath et al., 2001).

$$b_b(\lambda) = b_{bw}(\lambda) + b_{bp}(\lambda) \tag{5}$$

$$a_t(\lambda) = a_w(\lambda) + a_{dg}(\lambda) + a_{ph}(\lambda) \tag{6}$$

With $b_{bw}(\lambda)$ for the backscattering coefficient of pure seawater; $b_{bp}(\lambda)$ for the backscattering coefficient of particulate matter; $a_w(\lambda)$ for the absorption coefficient of pure seawater; $a_{dg}(\lambda)$ for the total absorption coefficient of non-pigmented particulate matter and colored dissolved organic matter; and $a_{ph}(\lambda)$ for the absorption coefficient of phytoplankton. Among them, $b_{bw}(\lambda)$ and $a_w(\lambda)$ can be considered known (Lee et al., 2015; Pope and Fry, 1997; Zhang et al., 2009); $b_{bp}(\lambda)$ can be modeled using Eq. (7), where η, the spectral power coefficient of $b_{bp}(\lambda)$, can be modeled using Eq. (8) (Wang et al., 2018); $a_{dg}(\lambda)$ can be modeled using Eq. (9), where S_{dg} is the spectral slope of $a_{dg}(\lambda)$ (Maritorena et al., 2002); and λ_0 is the reference wavelength nearest to 440 nm in Eq. (7) and Eq. (9). Through previous Gaussian parameters update, $a_{ph}(\lambda)$ can be modeled from aGau(435) and aGau(519) using Eq. (1). Therefore, R_{rs} spectrum can be modeled using Eqs. (1)–(9) with five variables (aGau (435), aGau(519), $b_{bp}(\lambda_0)$, $a_{dg}(\lambda_0)$, and S_{dg}).

$$b_{bp}(\lambda) = b_{bp}(\lambda_0)\left(\frac{\lambda_0}{\lambda}\right)^{\eta} \tag{7}$$

$$\eta = 2\left(1 - 1.2\exp\left(-0.9\frac{R_{rs}(440)}{R_{rs}(550)}\right)\right) \tag{8}$$

$$a_{dg}(\lambda) = a_{dg}(\lambda_0)\exp\left(-S_{dg}(\lambda_0 - 440)\right) \tag{9}$$

Fig. 2 (B) presents the overall flowchart of aGau(λ)s retrieval from R_{rs}, a spectral optimization procedure was adopted for retrieving these five unknowns (aGau(435), aGau(519), $b_{bp}(\lambda_0)$, $a_{dg}(\lambda_0)$, and S_{dg}) from HydroLight simulated/OLCI R_{rs} through minimizing the differences between them and the modeled R_{rs} spectra (Eqs. (1)–(9)), and the differences were also quantified by a target function same as that used by Wang et al. (2016). The retrieved aGau(435), aGau(519), and further $a_{ph}(\lambda_0)$ from HydroLight simulated and OLCI R_{rs} were then respectively used for the scheme construction and subsequent applications (separation of the origin of blooming phytoplankton in the offshore eddies). It should be noted that, to reduce noise impact of OLCI R_{rs}, we selected the average R_{rs} spectra value of 10 consecutive pixels for further spectral optimization and aGau(λ)s retrieval.

3.2. Scheme for separating the origin of blooming phytoplankton in offshore eddies

As described earlier, the phytoplankton communities or PFGs from offshore upwelling are different from those from nearshore waters, which can be represented by different combinations of phytoplankton pigments or the Gaussian peaks for phytoplankton absorption

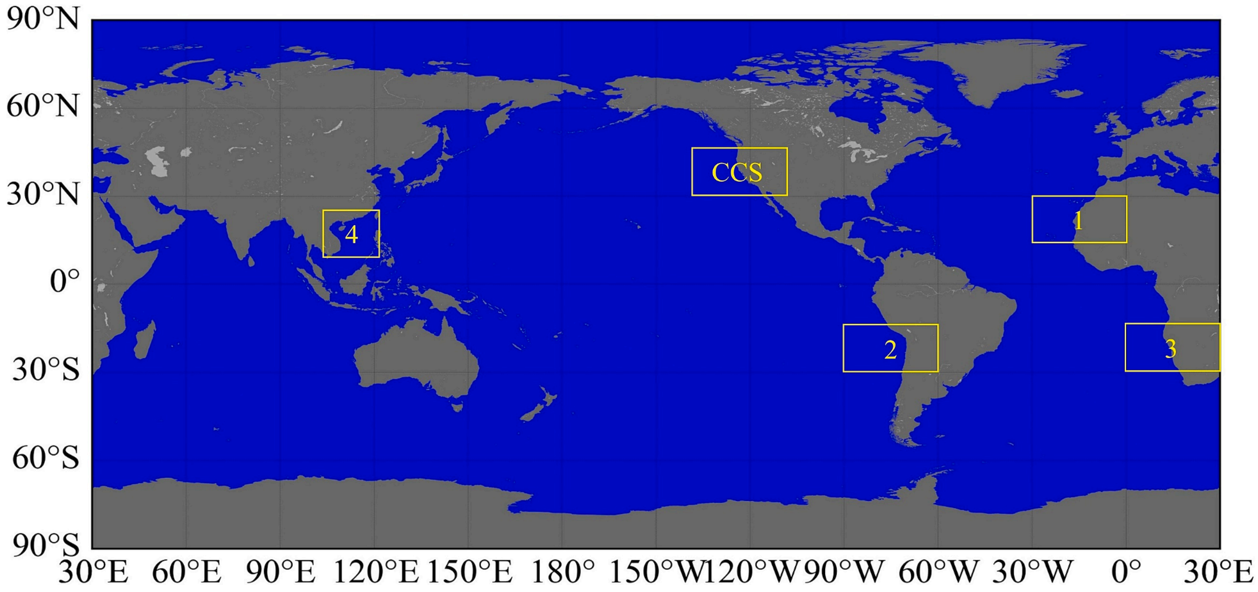

Fig. 3. The application regions of the scheme constructed in this study, which were framed with yellow rectangles and marked with characters. “CCS” represents the California Current System; “1” for the Canary Current System; “2” for the Peru–Chile Current System; “3” for the Benguela Current System; and “4” for the South China Sea and adjacent Taiwan Strait.

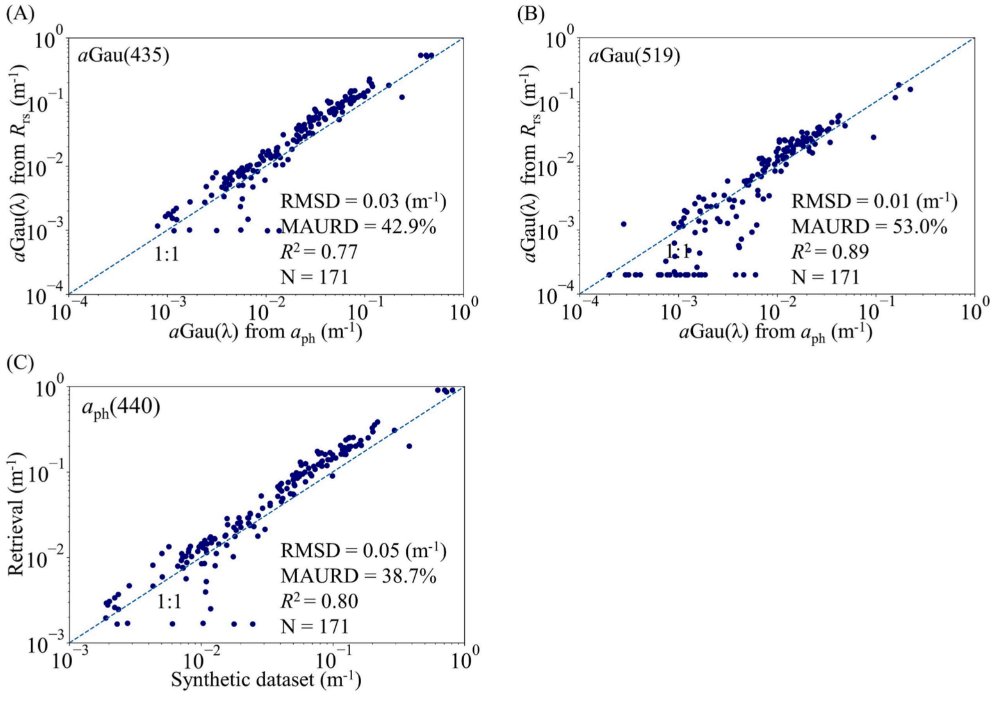

Fig. 4. (A) Scatterplot between aGau(435) decomposed from a_{ph} and that retrieved from R_{rs}. (B) Scatterplot between aGau(519) decomposed from a_{ph} and that retrieved from R_{rs}. (C) Scatterplot between $a_{\mathrm{ph}}(440)$ in the synthetic dataset and that retrieved from R_{rs}.

coefficient. To determine whether the absorption features are similar or not for blooming phytoplankton in the offshore eddies and that in the nearshore waters, Chla or phytoplankton absorption coefficient at a specific wavelength (e.g., 443 nm) alone are insufficient to distinguish different PFGs as they represent the overall biological or optical signals of the phytoplankton community. Furthermore, for a specific $a_{\mathrm{ph}}(443)$, the ratio of aGau(λ)s can indicate different compositions of pigments, and the latter can reveal the information of PFGs (Descy et al., 2009; Gieskes and Kraay, 1983; Mackey et al., 1996). Therefore, a two-dimensional spatial model, with $a_{\mathrm{ph}}(443)$ as one dimension and the ratio of aGau(λ)s as the other dimension, was proposed. We selected aGau(519)/aGau(435) as the indicator of different PFGs based on careful consideration of the following two factors: First, similar to using pigment ratios to indicate PFGs information (Aiken et al., 2007; Higgins and Mackey, 2000), the aGau(519)/aGau(435) could reveal the relative concentration of the accessory pigments to chlorophyll-a, and further provide content information for these accessory pigment-related PFGs (Chase et al., 2013). Specifically, aGau(519) represents the absorption Gaussian peak of photosynthetic carotenoids (PSC), including the pigments of 19′-hexanoyloxyfucoxanthin, fucoxanthin, 19′-butanoyloxyfucoxanthin, and peridinin, and they are the diagnostic pigments of haptophytes, diatoms, pelagophytes, and dinoflagellates, respectively

Table 2

Accuracy evaluation results between aGau(λ)s decomposed from a_{ph} and that retrieved from R_{rs} with the validation dataset.

Peak	Pigment	Gaussian peak center wavelength (nm)	MAURD (%)	RMSD (m^{-1})
1	Chl-a	380	52.3	0.06
2	Chl-a	415	46.6	0.03
3	Chl-a	435	42.9	0.03
4	Chl-c	457	35.0	0.03
5	PPC	488	35.6	0.02
6	PSC	519	53.0	0.01
7	PE	546	53.9	0.01
8	Chl-c	589	57.9	0.01
9	Chl-a	620	67.0	0.01
10	Chl-c	640	56.7	0.01
11	Chl-b	650	94.6	0.01
12	Chl-a	674	52.9	0.02
13	Chl-a	695	76.1	0.01

(Losa et al., 2017; Sun et al., 2018; Wang et al., 2018). aGau(435) represents the absorption peak of chlorophyll-a, therefore, for a given a_{ph}(443), separating aGau(519)/aGau(435) can indicate the differences of these PSC-related PFGs in the eddy and nearshore waters. Second, the retrieved aGau(519) and aGau(435) from R_{rs} have reliable accuracy, as described in detail in Section 4.1.

When this scheme was applied to OLCI R_{rs} data, we first retrieved aGau(435), aGau(519), and a_{ph}(443) with the updated MuPI model. Then, based on retrieved a_{ph}(443), we selected blooming phytoplankton in the eddy and nearshore waters, respectively. For the convenience of evaluation, the a_{ph}(443) values in these two areas should be similar. After that, scatterplots of these two areas were drawn between a_{ph}(443) and aGau(519)/aGau(435). Based on the clustering situation of the points in these two areas, we can determine whether they have similar origins, and finally separate upwelling from nearshore migrations of these offshore blooming eddies.

This scheme was subsequently applied to the California offshore waters, which is located in the CCS (marked as “CCS” in Fig. 3). In addition to the CCS, the scheme was applied to offshore waters associated with the Canary Current System (marked as number “1” in Fig. 3), the Peru–Chile Current System (number “2” in Fig. 3), the Benguela Current System (number “3” in Fig. 3), and the South China Sea and adjacent Taiwan Strait (number “4” in Fig. 3) to test its effectiveness.

3.3. Accuracy evaluation

To assess the performance of the updated MuPI model in retrieving aGau(λ)s from simulated R_{rs}, we used several accuracy evaluation metrics. These include the root mean squared difference (RMSD), mean absolute unbiased relative difference (MAURD), and coefficient of determination (R^2). The calculations for these metrics are as follows:

$$\mathrm{RMSD} = \sqrt{\frac{\sum_{i=1}^{N}(\widehat{y_i}-y_i)^2}{N}} \tag{10}$$

$$\mathrm{MAURD}\,(\%) = 200^{*}\frac{1}{N}\sum\nolimits_{i=1}^{N}\left|\frac{\widehat{y_i}-y_i}{y_i+\widehat{y_i}}\right| \tag{11}$$

$$R^2 = 1-\frac{\sum_{i=1}^{N}(y_i-\widehat{y_i})^2}{\sum_{i=1}^{N}(y_i-\overline{y_i})^2} \tag{12}$$

where y_i and $\widehat{y_i}$ represent the measured and retrieved results, respectively, $\overline{y_i}$ represents the average of the measurement results, and N is the number of matching data.

4. Results

4.1. Evaluation of the Gaussian peaks retrieval with the validation dataset

We first evaluated the performance of the updated MuPI model with the validation dataset described in Section 2.1, with results shown in Fig. 4. Specifically, Fig. 4 (A) presents the scatterplot between aGau (435) decomposed from a_{ph} spectra and that retrieved from R_{rs}, Fig. 4 (B) for aGau(519), we found that in the range of 10^{-4}–1.0 m^{-1}, most points were distributed near the 1:1 line. Fig. 4 (C) presents the points between the field-measured a_{ph}(440) and those retrieved from R_{rs}. For

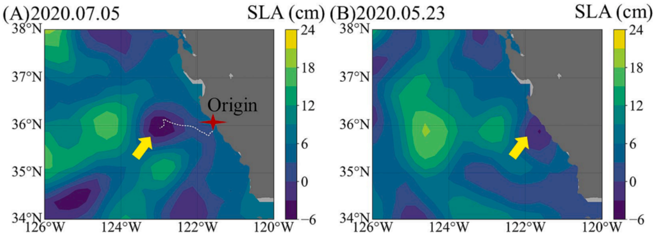

Fig. 6. (A) Sea level anomaly on July 5th, 2020, in the California offshore waters. The eddy was marked with a yellow arrow, the origin of the eddy was marked with a red star, and the approximate movement trajectory of the eddy was highlighted with a dashed white line. (B) Sea level anomaly on May 23rd, 2020, in the California offshore waters. The eddy was marked with a yellow arrow.

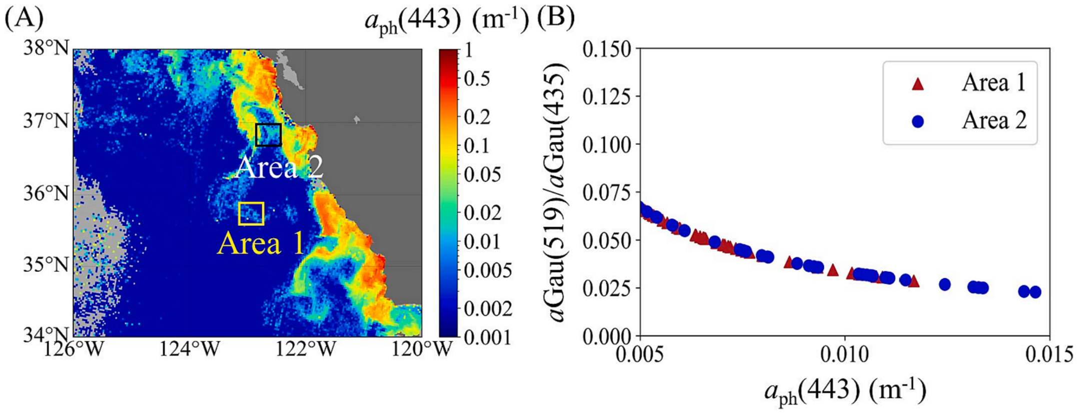

Fig. 5. (A) Distribution of a_{ph}(443) on July 5th, 2020, Area 1 (framed with a yellow rectangle, marked with yellow characters) represents blooming phytoplankton in the California offshore eddy, Area 2 (framed with a black rectangle, marked with white characters) represents blooming phytoplankton in the nearshore waters. (B) Scatterplot between a_{ph}(443) and ratio of aGau(519) and aGau(435) in Area 1 and Area 2. a_{ph}(443), aGau(435), and aGau(519) were retrieved from Ocean and Land Color Instrument R_{rs} data in the California offshore waters on July 5th, 2020.

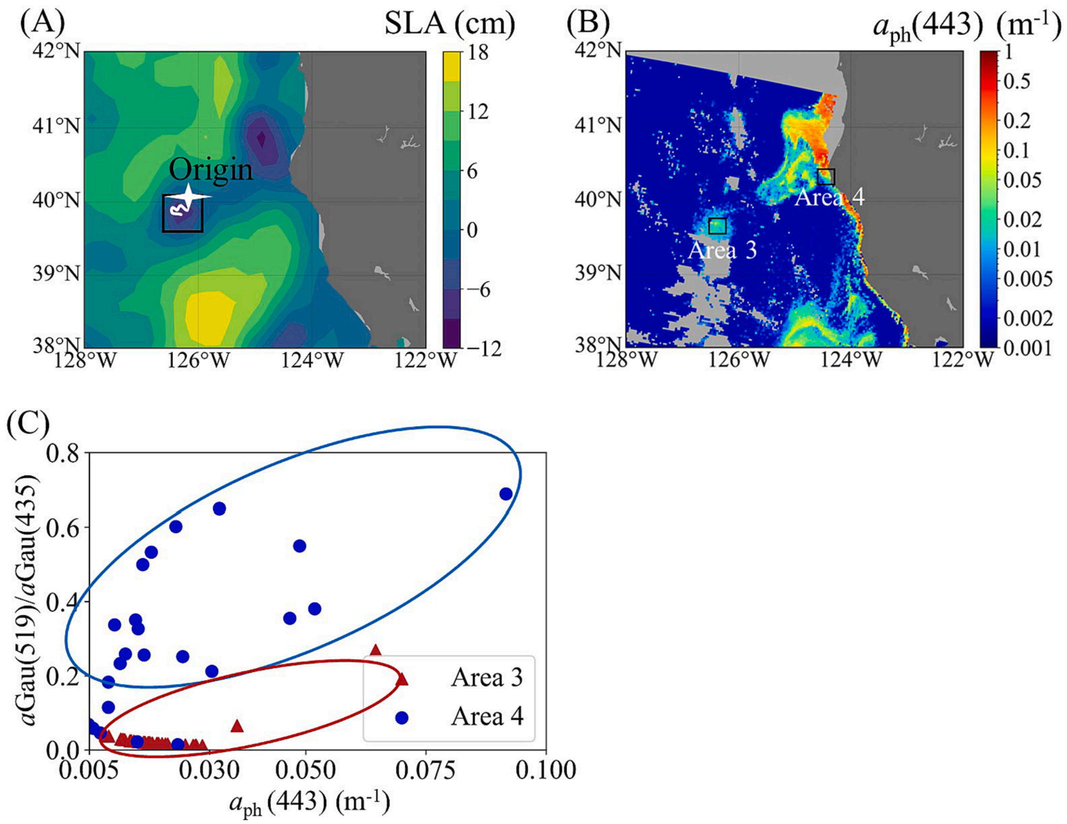

Fig. 7. (A) Sea level anomaly in the California offshore waters obtained using satellite altimeter on June 4th, 2017. The eddy was framed with a black rectangle, the origin of the eddy was marked with a white star, and the approximate movement trajectory of the eddy was highlighted with a solid white line. (B) Absorption coefficient of phytoplankton at 443 nm in the California offshore waters on June 4th, 2017. Area 3 (framed with a black rectangle, marked with white characters) represents blooming phytoplankton in the California offshore eddy, and Area 4 (framed with a black rectangle, marked with white characters) represents blooming phytoplankton in the nearshore waters. (C) Scatterplot between $a_{ph}(443)$ and the ratio of aGau(519) and aGau(435) of the California offshore eddy (Area 3) and nearshore waters (Area 4). Points framed with a red or blue ellipse indicate that they could be separated. $a_{ph}(443)$, aGau(435), and aGau(519) were retrieved from Ocean and Land Color Instrument R_{rs} data in the California offshore waters on June 4th, 2017.

$a_{ph}(440)$ in a range of 10^{-3}–1.0 m^{-1}, most points were also found distributed around the 1:1 line. As shown in Fig. 4 (A) and (B), we found that the aGau(435) and aGau(519) retrieved from R_{rs} were comparable to their values decomposed from a_{ph} (RMSD = 0.03 m^{-1}, MAURD = 42.9 %, $R^2 = 0.77$ for aGau(435); and RMSD = 0.01 m^{-1}, MAURD = 53.0 %, $R^2 = 0.89$ for aGau(519)), indicating that aGau(435) and aGau(519) retrieved from R_{rs} are in general reliable. In addition, the MAURD between aGau(519)/aGau(435) decomposed from a_{ph} and that retrieved from R_{rs} was found as 50.2 %, suggesting that the ratio retrieved from R_{rs} was generally close to that decomposed from a_{ph}. Further, for $a_{ph}(440)$ in a range of 10^{-3}–1.0 m^{-1} (see Fig. 4 (C)), $a_{ph}(440)$ retrieved from R_{rs} were also found in good agreement with known values, with RMSD = 0.05 m^{-1}, MAURD = 38.7 %, and $R^2 = 0.80$. These results suggest that the updated MuPI model is suitable for the retrieval of aGau(435), aGau(519), and $a_{ph}(440)$ from R_{rs} for different water environments, and using the retrieved aGau(519)/aGau(435) from R_{rs} as an index to separate the origin of blooming phytoplankton in the offshore eddies is feasible.

We also compared the accuracies of all 13 Gaussian peaks decomposed from a_{ph} spectra and those retrieved from R_{rs}, with the results presented in Table 2. In the column of pigment, Chl is chlorophyll, PPC is photoprotective carotenoid, PSC is photosynthetic carotenoid, and PE is phycoerythrin. We found that the aGau(λ)s retrieved from R_{rs} were close to their values decomposed from a_{ph}, with the MAURDs for most aGau(λ)s less than 60 %, and the RMSDs for all aGau(λ)s not more than 0.06 m^{-1}, where aGau(λ)s were as high as $\sim$ 0.5 m^{-1}.

4.2. Local growth or migration of blooming phytoplankton in a California offshore eddy

The scheme to separate the origin of blooming phytoplankton in offshore eddies has been described in detail in Section 3.2, which was then applied to California offshore R_{rs} data obtained by OLCI on July 5th, 2020. The retrieved $a_{ph}(443)$ from OLCI R_{rs} are presented in Fig. 5 (A), where the distribution of $a_{ph}(443)$ is similar to that of Chla (Fig. 1 (A)), as both are indicators of phytoplankton. The selected blooming phytoplankton in the eddy and nearshore waters were framed with yellow (Area 1) and black (Area 2) rectangles, respectively. As we focused on blooming phytoplankton in the eddy, a threshold of 0.005 m^{-1} was set for $a_{ph}(443)$, and waters with $a_{ph}(443)$ values less than this threshold were not considered. The scatterplot between $a_{ph}(443)$ and aGau(519)/aGau(435) in these two selected areas is presented in Fig. 5 (B), we found that most points were overlapped, with cosine similarity of 0.99, and pearson correlation coefficient of 0.97 ($P < 0.001$), i.e., they showed similar dependences, suggesting that the blooming phytoplankton in the eddy might be a result of the migration of high Chla nearshore waters.

This conclusion, based on ocean color remote sensing, was verified using daily SLA data, with the results shown in Fig. 6 (A), where a notable negative anomaly was observed on July 5th, 2020 (marked with a yellow arrow), indicating that the eddy we detected was a cyclone eddy. We then traced the eddy's daily movement trajectory backward, the origin of the eddy was marked with a red star, and the approximate movement trajectory was highlighted with a dashed white line in Fig. 6 (A). As shown in Fig. 6 (B), the eddy was found originated from the

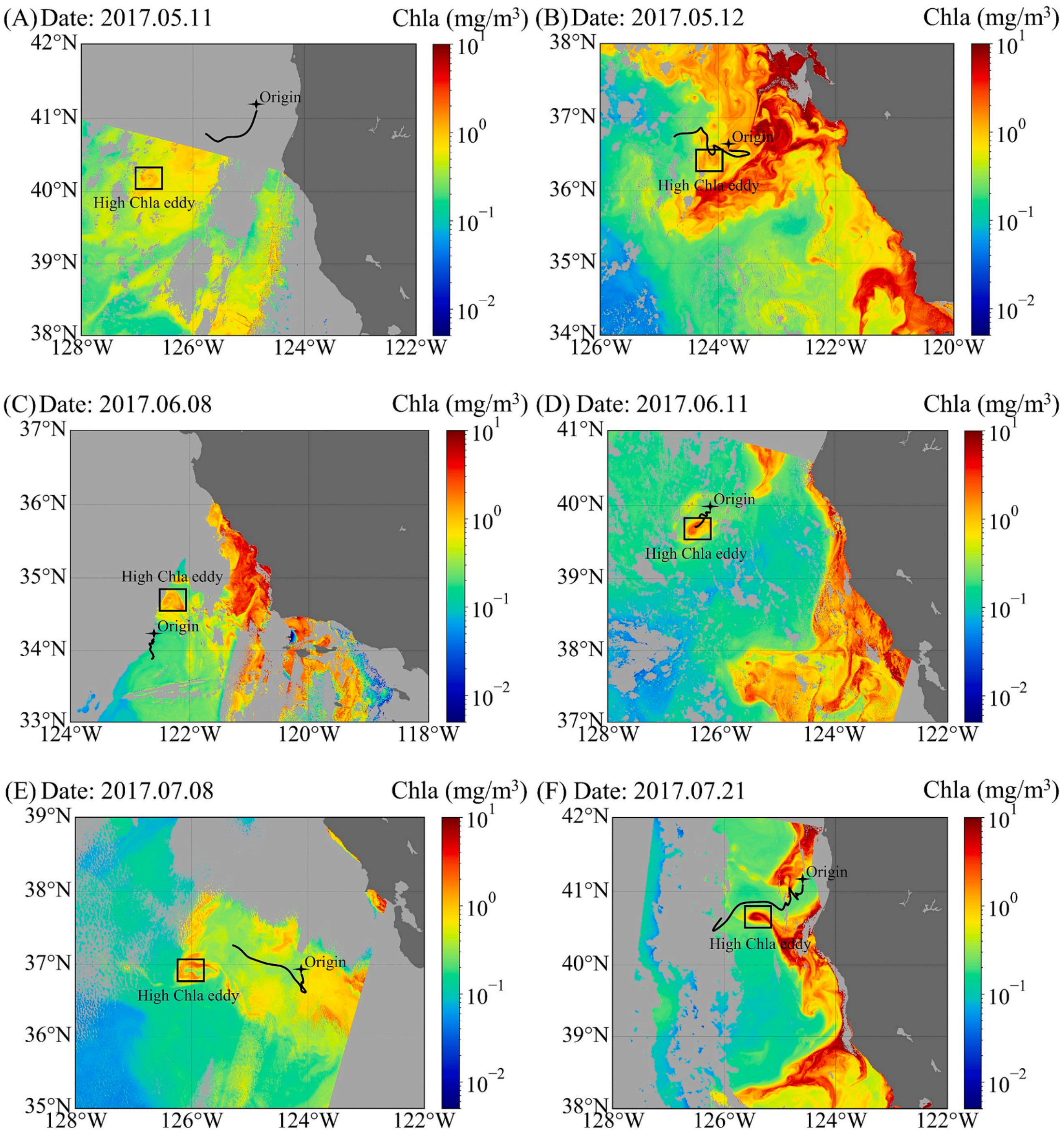

Fig. 8. Six images of chlorophyll-a concentration in the California offshore waters on different dates during the spring and summer of 2017. The eddies were framed with black rectangles and marked nearby. The origins of these eddies were marked with black stars, and the approximate movement trajectories of these eddies were highlighted with solid black lines.

nearshore region on about May 23rd, 2020 (marked with a yellow arrow). This result is consistent with that obtained from ocean color remote sensing for this high Chla offshore eddy.

4.3. Blooming phytoplankton in an eddy by local growth

Furthermore, an eddy in the California offshore on June 4th, 2017 (Fig. 7 (A), framed with a black rectangle) was utilized to demonstrate the identification of blooming phytoplankton in an eddy that is due to local growth. Through daily SLA data, the eddy was found formed in the California offshore on about May 25th, 2017 (see the white star in Fig. 7 (A), with the solid white line showing its approximate movement trajectory). The $a_{ph}(443)$ values retrieved from R_{rs}, as depicted in Fig. 7 (B), also revealed a distinct eddy imprint, which is consistent with the detection results from the SLA data and the Chla distribution presented in Fig. 1 (B). We also selected two areas (Area 3 and Area 4, framed with black rectangles), then used our scheme to classify the origin of blooming phytoplankton present in the eddy, with results presented in Fig. 7 (C). Overall, the points associated with Area 3 and Area 4 were found clustered quite separately (framed with red and blue ellipses, respectively). While both areas had similar $a_{ph}(443)$ (i.e., similar Chla), with the average value of $a_{ph}(443)$ in Area 3 was 0.020 m^{-1}, and the average value of $a_{ph}(443)$ in Area 4 was 0.023 m^{-1}. The different clusters suggest that the phytoplankton in these two areas are different in PFGs, indicating that they have different origins. This was also supported by the trajectory of this eddy over the previous ~ 10 days.

5. Discussion

5.1. More examples of separating blooming phytoplankton associated with offshore eddies

In the above section, examples were presented to identify blooming phytoplankton in offshore eddies from the migration of nearshore waters or local growth. To further evaluate our separation scheme, we selected six more images that displayed clear eddy patterns in the California offshore in the spring and summer (March to August) of 2017; and the dates and locations of these eddies (see black rectangles) are

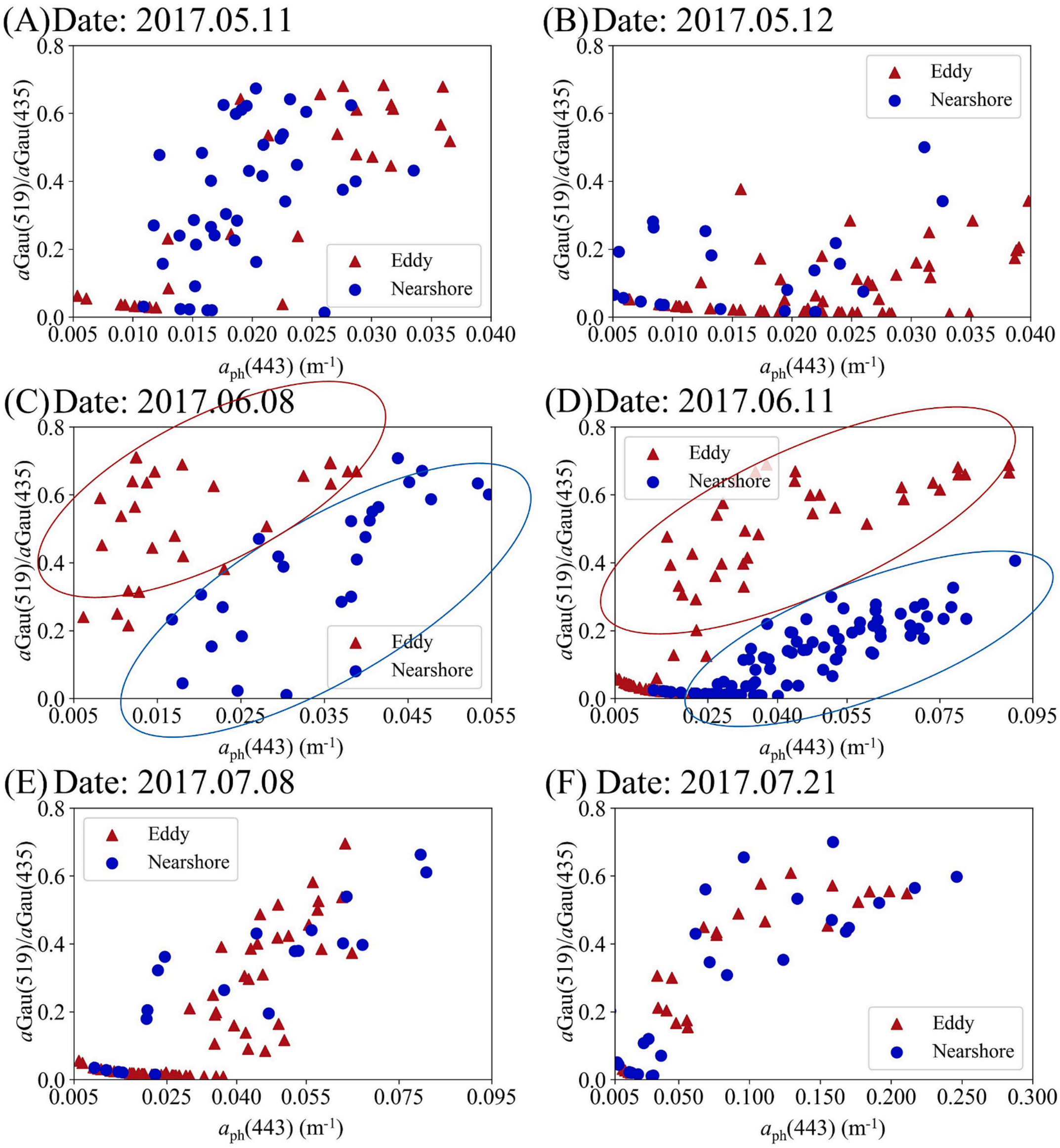

Fig. 9. Scatterplots between $a_{ph}(443)$ and ratio of aGau(519) and aGau(435) of blooming phytoplankton in the California offshore eddy and nearshore waters on different dates during the spring and summer of 2017. Points framed with a red or blue ellipse indicate that they could be separated. $a_{ph}(443)$, aGau(435), and aGau (519) were retrieved from Ocean and Land Color Instrument R_{rs} data on different dates in the offshore waters of California.

presented in Fig. 8. According to the eddy movement trajectory detected using the SLA data, the origins of these eddies were marked with black stars, and the approximate movement trajectories of these eddies were highlighted with solid black lines (Fig. 8). Although some locations of blooming phytoplankton in the eddies observed through Chla images were not consistent with the locations of the cores of eddies detected using SLA data, these satellite altimeters detected cores of eddies that were closest to the blooming phytoplankton waters on the same day, and the eddies had a certain area, with a horizontal scale of tens to hundreds of kilometers; thus, the blooming phytoplankton were still affected by the eddies detected through satellite altimetry. Following the movement trajectory revealed by the SLA data, blooming phytoplankton in the eddies in Fig. 8 (A) and (F) (date: 2017.05.11 and 2017.07.21) originated from nearshore, while the blooming phytoplankton in the eddies in Fig. 8 (B), (C), (D), and (E) (date: 2017.05.12, 2017.06.08, 2017.06.11, and 2017.07.08) originated from local growth.

The relationship between $a_{ph}(443)$ and aGau(519)/aGau(435) for blooming phytoplankton in the eddy and nearshore waters is shown in Fig. 9, which corresponds to the multiple subgraphs in Fig. 8. According to the eddy trajectories detected using the SLA data, the blooming phytoplankton associated with eddies originating from the nearshore correspond to Fig. 9 (A) and (F), and the blooming phytoplankton in the eddies originating from local growth correspond to Fig. 9 (B), (C), (D), and (E). Therefore, as shown in Fig. 9, our scheme correctly separated the origin of blooming phytoplankton in the eddies corresponding to Fig. 9 (A), (C), (D), and (F), but could not identify the origin of blooming phytoplankton in the eddies corresponding to Fig. 9 (B) and (E). Specifically, as shown in Fig. 9 (A) and (F), the points of eddy and nearshore waters clustered together, which were difficult to separate, suggesting that the blooming phytoplankton in the eddies had similar community structures as that from nearshore waters. For those shown in Fig. 9 (C) and (D), the points of the eddy and nearshore waters were clustered separately (framed with red and blue ellipses, respectively), indicating that they can be separated through this two-dimensional space; in other words, the blooming phytoplankton in these eddies were determined to originate from local growth. However, no obvious separation of clustering points was found for the eddy and nearshore waters in Fig. 9 (B) and (E), indicating that this scheme cannot identify the origins of

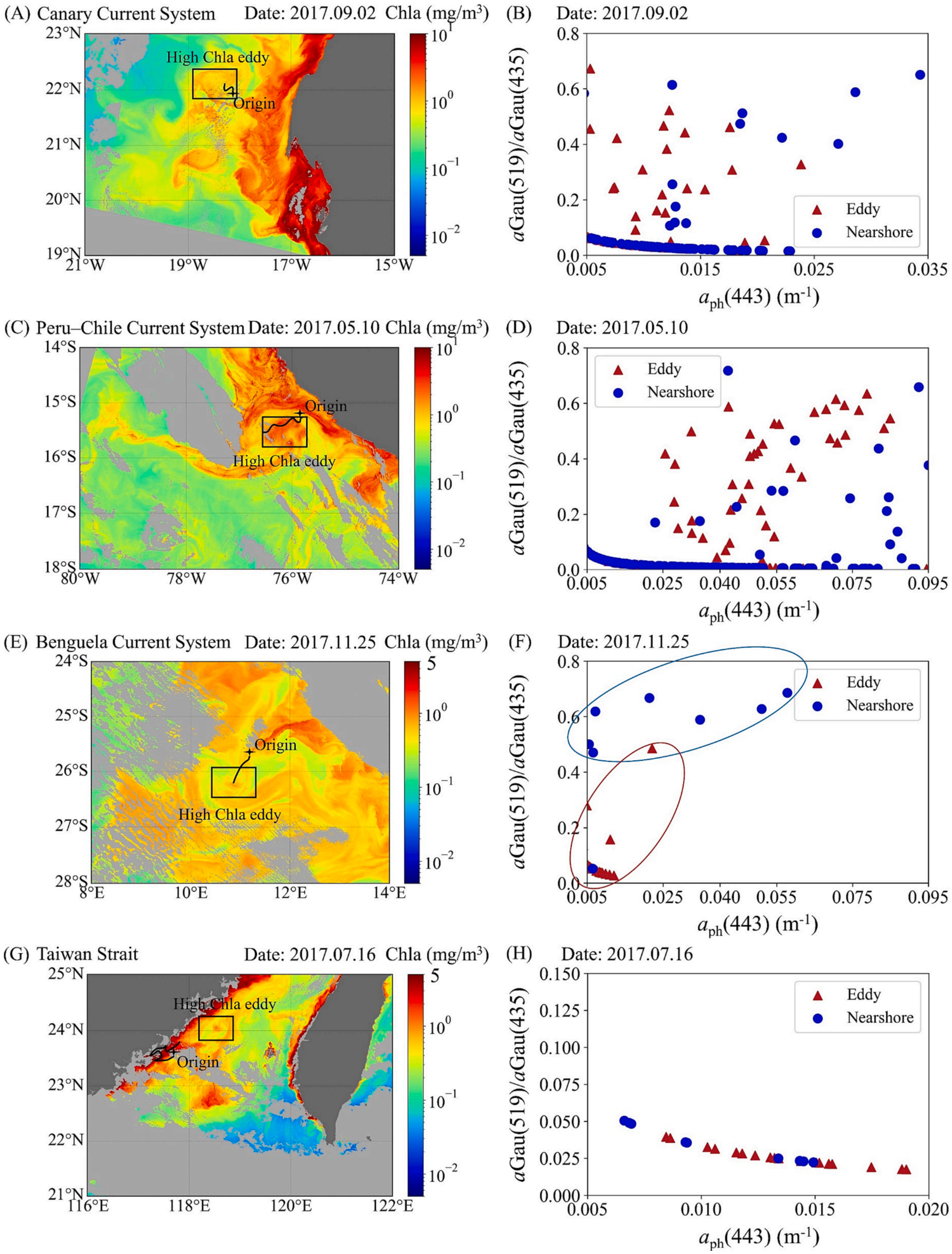

Fig. 10. Chlorophyll-a concentration images in the (A) Canary Current System, (C) Peru–Chile Current System, (E) Benguela Current System, and (G) South China Sea and adjacent Taiwan Strait. The blooming phytoplankton in these eddies were framed with black rectangles and marked nearby, the origins of these eddies were marked with black stars, and the approximate movement trajectories of these eddies were highlighted with solid black lines. Scatterplots between $a_{ph}(443)$ and ratio of aGau(519) and aGau(435) in the eddies and nearshore waters in (B) Canary Current System, (D) Peru–Chile Current System, (F) Benguela Current System, and (H) South China Sea and adjacent Taiwan Strait. Points framed with a red or blue ellipse indicate that they could be separated. $a_{ph}(443)$, aGau(435), and aGau(519) were retrieved from Ocean and Land Color Instrument R_{rs} data on different dates in the offshore waters in these areas.

blooming phytoplankton (local growth) in these two eddies. Based on these detection results and those on June 4th, 2017 (see Section 4.3), our scheme successfully separated 71 % of the origins of blooming phytoplankton in the California offshore eddies during the spring and summer of 2017.

5.2. *Separating the origin of blooming phytoplankton in other offshore waters*

In addition to apply our scheme to California offshore waters, we also evaluated the applicability of this scheme to other offshore waters, as mentioned in Section 2.2 and Section 3.2, with the results shown in Fig. 10. The subgraphs in the left half of the figure are the Chla images in these areas on different dates; the blooming phytoplankton in these eddies were framed with black rectangles and marked nearby, through satellite altimetry, the origins of these eddies were marked with black stars, and the approximate movement trajectories of these eddies were highlighted with solid black lines. Based on the eddy movement trajectory, we found that the blooming phytoplankton in the eddies in Fig. 10 (A), (C), and (G) originated from the nearshore, and the blooming phytoplankton in the eddy in Fig. 10 (E) originated from local growth. The subgraphs in the right panel of Fig. 10 show the corresponding relationships between $a_{\mathrm{ph}}(443)$ and $a\mathrm{Gau}(519)/a\mathrm{Gau}(435)$ in the eddy and nearshore waters in these areas. We found that the points in Fig. 10 (B), (D), and (H) were clustered together in different water areas, suggesting that they were determined to originate from nearshore waters, while the points from eddy and nearshore waters were clustered separately in Fig. 10 (F), indicating that they were determined to originate from local growth, which is consistent with the origins detected through the SLA data. These results further support the scheme in identifying the origins of blooming phytoplankton in these eddies.

5.3. *Applicability and limitations of our scheme*

In this study, we proposed a scheme with a two-dimensional spatial model to separate the origin of blooming phytoplankton (i.e., migration from the nearshore or local growth) in the offshore eddies from satellite ocean color measurements. This scheme showed satisfactory success in classifying the origin of blooming phytoplankton in eddies in the California and other offshore waters with OLCI R_{rs}. Aiken et al. (2009) separated different phytoplankton size classes using a two-dimensional pigment space, with total Chla (TChla) as one dimension, and either the ratio of TChla and accessory pigment concentration (TChla/AP) or the ratio of photoprotective carotenoid concentration and total carotenoid concentration (PPC/TC) as the other dimension. These two schemes are similar in concept, although we did not identify specific phytoplankton size class such as microplankton.

As all remote sensing algorithms, there are some limitations of our scheme. First, as we focus on the blooming phytoplankton in the offshore eddies with higher Chla; thus, in our scheme, there is a lower threshold and was set as $a_{\mathrm{ph}}(443) = 0.005\ \mathrm{m}^{-1}$, that means for weak “blooms”, this scheme in its current form will not be applicable. Second, to ensure that the offshore eddy area could be evaluated using nearshore high Chla waters, it is necessary for the nearshore region to have similar $a_{\mathrm{ph}}(443)$ as that of offshore eddy waters. Third, the merging of eddies is frequent in the ocean (Cui et al., 2019), which may result in changes of phytoplankton community structure, making it more challenging to identify the origin of blooming phytoplankton in the offshore eddies with the present form of this scheme. Finally, the quality of R_{rs} is the key to the retrieval of $a_{\mathrm{ph}}(443)$ and aGau(519)/aGau(435); presently, we do not have a broadly accepted scheme to mask out low-quality OLCI R_{rs}. All of these should be updated or further improved down the road.

6. Summary

In this study, we updated the MuPI model for retrieving a_{ph} and $a\mathrm{Gau}(\lambda)$s from an R_{rs} spectrum for different aquatic environments. More importantly, we proposed an innovative scheme for identifying the origin of blooming phytoplankton in the offshore eddies using satellite ocean color measurements. In this scheme, a two-dimensional space formed by $a_{\mathrm{ph}}(443)$ and $a\mathrm{Gau}(519)/a\mathrm{Gau}(435)$ is used to determine whether the blooming phytoplankton in the eddy and nearshore waters have similar PFGs, and this similarity, or not, is used to judge the origin of blooming phytoplankton in the offshore eddies. The test and validation of this scheme indicated that it has an overall accuracy of over 71 % for identifying the origin of blooming phytoplankton in the offshore eddies over various regions. This scheme broadens the application of satellite ocean color measurements from traditional biogeochemical studies to offshore eddy dynamics.

CRediT authorship contribution statement

Qing Zhu: Conceptualization, Methodology, Writing – original draft, Writing – review & editing. **Zhongping Lee:** Conceptualization, Funding acquisition, Methodology, Writing – review & editing.

Declaration of competing interest

The authors declare that they have no known competing financial interests or personal relationships that could have appeared to influence the work reported in this paper.

Data availability

Data will be made available on request.

Acknowledgments

This work was financially supported by the National Natural Science Foundation of China (#42250710150, #41830102, #41890803, #41941008). Qing Zhu was supported by the Outstanding Postdoctoral Scholarship of the State Key Laboratory of Marine Environmental Science at Xiamen University. We thank NASA Goddard Space Flight Center for providing OLCI data, thank CMEMS for providing SLA data, and are grateful to those scientific researchers for sharing field measurements via NASA SeaBASS. Comments and suggestions from two anonymous reviewers are greatly appreciated.

Appendix A. Supplementary material

Supplementary data to this article can be found online at https://doi.org/10.1016/j.pocean.2024.103232.

References

Aiken, J., Fishwick, J.R., Lavender, S., Barlow, R., Moore, G.F., Sessions, H., Bernard, S., Ras, J., Hardman-Mountford, N.J., 2007. Validation of MERIS reflectance and chlorophyll during the BENCAL cruise October 2002: preliminary validation of new demonstration products for phytoplankton functional types and photosynthetic parameters. Int. J. Remote Sens. 28 (3–4), 497–516. https://doi.org/10.1080/01431160600821036.

Aiken, J., Pradhan, Y., Barlow, R., Lavender, S., Poulton, A., Holligan, P., Hardman-Mountford, N., 2009. Phytoplankton pigments and functional types in the Atlantic Ocean: a decadal assessment, 1995–2005. Deep Sea Res. Part II: Topical Stud. Oceanogr. 56 (15), 899–917. https://doi.org/10.1016/j.dsr2.2008.09.017.

Amores, A., Melnichenko, O., Maximenko, N., 2017. Coherent mesoscale eddies in the North Atlantic subtropical gyre: 3-D structure and transport with application to the salinity maximum. J. Geophys. Res. Oceans 122 (1), 23–41. https://doi.org/10.1002/2016JC012256.

Amos, C.M., Castelao, R.M., Medeiros, P.M., 2019. Offshore transport of particulate organic carbon in the California current system by mesoscale eddies. Nat. Commun. 10 (1), 4940. https://doi.org/10.1038/s41467-019-12783-5.

Batten, S.D., Crawford, W.R., 2005. The influence of coastal origin eddies on oceanic plankton distributions in the eastern Gulf of Alaska. Deep Sea Res. Part II: Topical Stud. Oceanogr. 52 (7–8), 991–1009. https://doi.org/10.1016/j.dsr2.2005.02.009.

Benitez-Nelson, C.R., Bidigare, R.R., Dickey, T.D., Landry, M.R., Leonard, C.L., Brown, S. L., Nencioli, F., Rii, Y.M., Maiti, K., Becker, J.W., Bibby, T.S., Black, W., Cai, W.-J., Carlson, C.A., Chen, F., Kuwahara, V.S., Mahaffey, C., McAndrew, P.M., Quay, P.D., Rappé, M.S., Selph, K.E., Simmons, M.P., Yang, E.J., 2007. Mesoscale eddies drive increased silica export in the subtropical Pacific Ocean. Science 316 (5827), 1017–1021. https://doi.org/10.1126/science.1136221.

Bidigare, R. R., Ondrusek, M. E., Morrow, J. H., Kiefer, D. A. 1990, In vivo absorption properties of algal pigments. Proc. SPIE, 1302, Ocean Optics X. https://doi.org/10.1117/12.21451.

Bricaud, A., Claustre, H., Ras, J., Oubelkheir, K., 2004. Natural variability of phytoplanktonic absorption in oceanic waters: influence of the size structure of algal populations. J. Geophys. Res. 109 (C11), 1–12. https://doi.org/10.1029/2004JC002419.

Chaigneau, A., Eldin, G., Dewitte, B., 2009. Eddy activity in the four major upwelling systems from satellite altimetry (1992–2007). Prog. Oceanogr. 83 (1–4), 117–123. https://doi.org/10.1016/j.pocean.2009.07.012.

Chase, A., Boss, E., Zaneveld, R., Bricaud, A., Claustre, H., Ras, J., Dall'Olmo, G., Westberry, T.K., 2013. Decomposition of in situ particulate absorption spectra. Methods Oceanogr. 7, 110–124. https://doi.org/10.1016/j.mio.2014.02.002.

Chelton, D.B., Schlax, M.G., Samelson, R.M., de Szoeke, R.A., 2007. Global observations of large oceanic eddies. Geophys. Res. Lett. 34 (15), 87–101. https://doi.org/10.1029/2007GL030812.

Chelton, D.B., Gaube, P., Schlax, M.G., Early, J.J., Samelson, R.M., 2011a. The influence of nonlinear mesoscale eddies on near-surface oceanic chlorophyll. Science 334 (6054), 328–332. https://doi.org/10.1126/science.1208897.

Chelton, D.B., Schlax, M.G., Samelson, R.M., 2011b. Global observations of nonlinear mesoscale eddies. Prog. Oceanogr. 91 (2), 167–216. https://doi.org/10.1016/j.pocean.2011.01.002.

Chen, Y., Tang, D., 2012. Eddy-feature phytoplankton bloom induced by a tropical cyclone in the South China Sea. Int. J. Remote Sens. 33 (23), 7444–7457. https://doi.org/10.1080/01431161.2012.685976.

Chen, Y., Qiu, D., Cornillon, P., Wu, M., 2022. Chlorophyll bloom enhanced by a mesoscale eddy in the western South China Sea. Front. Earth Sci. 1–8 https://doi.org/10.1007/s11707-022-0984-3.

Chenillat, F., Franks, P.J.S., Rivière, P., Capet, X., Grima, N., Blanke, B., 2015. Plankton dynamics in a cyclonic eddy in the Southern California current system. J. Geophys. Res. Oceans 120 (8), 5566–5588. https://doi.org/10.1002/2015JC010826.

Cui, W., Wang, W., Zhang, J., Yang, J., 2019. Multicore structures and the splitting and merging of eddies in global oceans from satellite altimeter data. Ocean Sci. 15 (2), 413–430. https://doi.org/10.5194/os-15-413-2019.

Descy, J.-P., Sarmento, H., Higgins, H.W., 2009. Variability of phytoplankton pigment ratios across aquatic environments. Eur. J. Phycol. 44 (3), 319–330. https://doi.org/10.1080/09670260802618942.

Dong, C., McWilliams, J.C., Liu, Y., Chen, D., 2014. Global heat and salt transports by eddy movement. Nat. Commun. 5 (1), 3294. https://doi.org/10.1038/ncomms4294.

Falkowski, P.G., Ziemann, D., Kolber, Z., Bienfang, P.K., 1991. Role of eddy pumping in enhancing primary production in the ocean. Nature 352 (6330), 55–58. https://doi.org/10.1038/352055a0.

Frenger, I., Münnich, M., Gruber, N., 2018. Imprint of Southern Ocean mesoscale eddies on chlorophyll. Biogeosciences 15 (15), 4781–4798. https://doi.org/10.5194/bg-15-4781-2018.

Gaube, P., Chelton, D.B., Strutton, P.G., Behrenfeld, M.J., 2013. Satellite observations of chlorophyll, phytoplankton biomass, and Ekman pumping in nonlinear mesoscale eddies. J. Geophys. Res. Oceans 118 (12), 6349–6370. https://doi.org/10.1002/2013JC009027.

Gaube, P., McGillicuddy, D.J., Chelton, D.B., Behrenfeld, M.J., Strutton, P.G., 2014. Regional variations in the influence of mesoscale eddies on near-surface chlorophyll. J. Geophys. Res. Oceans 119 (12), 8195–8220. https://doi.org/10.1002/2014JC010111.

Gieskes, W.W.C., Kraay, G.W., 1983. Dominance of cryptophyceae during the phytoplankton spring bloom in the Central North Sea detected by HPLC analysis of pigments. Mar. Biol. 75 (2), 179–185. https://doi.org/10.1007/BF00406000.

Gordon, H.R., Brown, O.B., Evans, R.H., Brown, J.W., Smith, R.C., Baker, K.S., Clark, D. K., 1988. A semianalytic radiance model of ocean color. J. Geophys. Res. Atmos. 93 (D9), 10909–10924. https://doi.org/10.1029/JD093iD09p10909.

Hausmann, U., Czaja, A., 2012. The observed signature of mesoscale eddies in sea surface temperature and the associated heat transport. Deep Sea Res. Part I: Oceanogr. Res. Papers. 70, 60–72. https://doi.org/10.1016/j.dsr.2012.08.005.

He, Q., Zhan, H., Shuai, Y., Cai, S., Li, Q.P., Huang, G., Li, J., 2017. Phytoplankton bloom triggered by an anticyclonic eddy: the combined effect of eddy-Ekman pumping and winter mixing. J. Geophys. Res. Oceans 122 (6), 4886–4901. https://doi.org/10.1002/2017JC012763.

He, Q., Zhan, H., Cai, S., Zhan, W., 2021. Eddy-induced near-surface chlorophyll anomalies in the subtropical gyres: biomass or physiology? Geophys. Res. Lett. 48 (7), 1–10. https://doi.org/10.1029/2020GL091975.

Higgins, H.W., Mackey, D.J., 2000. Algal class abundances, estimated from chlorophyll and carotenoid pigments, in the western Equatorial Pacific under El Niño and non-El Niño conditions. Deep Sea Res. Part I: Oceanogr. Res. Papers. 47 (8), 1461–1483. https://doi.org/10.1016/S0967-0637(99)00114-4.

Hoepffner, N., Sathyendranath, S., 1991. Effect of pigment composition on absorption properties of phytoplankton. Mar. Ecol. Prog. Ser. 73 (1), 11–23. https://doi.org/10.3354/meps073011.

Hong, T.T.M., Park, Y.-G., Choi, J.M., 2023. Divergence observation in a mesoscale eddy during chla bloom revealed in submesoscale satellite currents. Remote Sens. (Basel) 15 (4), 995. https://doi.org/10.3390/rs15040995.

Huang, B., Hu, J., Xu, H., Cao, Z., Wang, D., 2010. Phytoplankton community at warm eddies in the northern South China Sea in winter 2003/2004. Deep Sea Res. Part II: Topical Stud. Oceanogr. 57 (19–20), 1792–1798. https://doi.org/10.1016/j.dsr2.2010.04.005.

IOCCG, 2006. Remote sensing of inherent optical properties: fundamentals, tests of algorithms, and applications. In: Lee, Z.-P. (Ed.), Reports of the International Ocean-Colour Coordinating Group, No. 5. IOCCG, Dartmouth, Canada.

IOCCG-OCAG, 2003. Models, parameters, and approaches that used to generate wide range of absorption and backscattering spectra. International Ocean-Colour Coordinating Group.

Jeffrey, S.W., Wright, S.W., Zapata, M., 2011. Microalgal classes and their signature pigments. In: Roy, S., Llewellyn, C.A., Egeland, E.S., Johnsen, G. (Eds.), Phytoplankton Pigments: Characterization, Chemotaxonomy, and Application in Oceanography. Cambridge University Press, Cambridge, United Kingdom, pp. 3–77. https://doi.org/10.1017/CBO9780511732263.004.

Klein, P., Lapeyre, G., 2009. The oceanic vertical pump induced by mesoscale and submesoscale turbulence. Ann. Rev. Mar. Sci. 1, 351–375. https://doi.org/10.1146/annurev.marine.010908.163704.

Krause, J.W., Brzezinski, M.A., Largier, J.L., McNair, H.M., Maniscalco, M., Bidle, K.D., Allen, A.E., Thamatrakoln, K., 2020. The interaction of physical and biological factors drives phytoplankton spatial distribution in the northern California current. Limnol. Oceanogr. 65 (9), 1974–1989. https://doi.org/10.1002/lno.11431.

Kurian, J., Colas, F., Capet, X., McWilliams, J.C., Chelton, D.B., 2011. Eddy properties in the California current system. J. Geophys. Res. Oceans 116 (C8), 1–18. https://doi.org/10.1029/2010JC006895.

Ladd, C., Kachel, N.B., Mordy, C.W., Stabeno, P.J., 2005. Observations from a Yakutat eddy in the northern Gulf of Alaska. J. Geophys. Res. Oceans 110 (C3), 1–11. https://doi.org/10.1029/2004JC002710.

Laiolo, L., McInnes, A.S., Matear, R., Doblin, M.A., 2016. Key drivers of seasonal plankton dynamics in cyclonic and anticyclonic eddies off East Australia. Front. Mar. Sci. 3, 155. https://doi.org/10.3389/fmars.2016.00155.

Lee, Z., Carder, K.L., Arnone, R.A., 2002. Deriving inherent optical properties from water color: a multiband quasi-analytical algorithm for optically deep waters. Appl. Opt. 41 (27), 5755–5772. https://doi.org/10.1364/AO.41.005755.

Lee, Z., Wei, J., Voss, K., Lewis, M., Bricaud, A., Huot, Y., 2015. Hyperspectral absorption coefficient of "pure" seawater in the range of 350–550 nm inverted from remote sensing reflectance. Appl. Opt. 54 (3), 546–558. https://doi.org/10.1364/AO.54.000546.

Lee, Z., Shang, S., Du, K., Wei, J., 2018. Resolving the long-standing puzzles about the observed Secchi depth relationships. Limnol. Oceanogr. 63 (6), 2321–2336. https://doi.org/10.1002/lno.10940.

Lee, Z., Shang, S., Du, K., Lin, G., Liu, T., Zoffoli, L., 2019. Estimating the transmittance of visible solar radiation in the upper ocean using Secchi disk observations. J. Geophys. Res. Oceans 124 (3), 1434–1444. https://doi.org/10.1029/2018JC014543.

Lehahn, Y., d'Ovidio, F., Lévy, M., Amitai, Y., Heifetz, E., 2011. Long range transport of a quasi isolated chlorophyll patch by an Agulhas ring. Geophys. Res. Lett. 38 (16), 1–6. https://doi.org/10.1029/2011GL048588.

Lin, I.-I., Lien, C.-C., Wu, C.-R., Wong, G.T.F., Huang, C.-W., Chiang, T.-L., 2010. Enhanced primary production in the oligotrophic South China Sea by eddy injection in spring. Geophys. Res. Lett. 37 (16), 1–5. https://doi.org/10.1029/2010GL043872.

Losa, S.N., Soppa, M.A., Dinter, T., Wolanin, A., Brewin, R.J.W., Bricaud, A., Oelker, J., Peeken, I., Gentili, B., Rozanov, V., Bracher, A., 2017. Synergistic exploitation of hyper- and multi-spectral precursor sentinel measurements to determine phytoplankton functional types (SynSenPFT). Front. Mar. Sci. 4, 203. https://doi.org/10.3389/fmars.2017.00203.

Mackey, M.D., Mackey, D.J., Higgins, H.W., Wright, S.W., 1996. CHEMTAX - a program for estimating class abundances from chemical markers: application to HPLC measurements of phytoplankton. Mar. Ecol. Prog. Ser. 144, 265–283. https://doi.org/10.3354/meps144265.

Maritorena, S., Siegel, D.A., Peterson, A.R., 2002. Optimization of a semianalytical ocean color model for global-scale applications. Appl. Opt. 41 (15), 2705–2714. https://doi.org/10.1364/AO.41.002705.

McGillicuddy, D.J., Robinson, A.R., Siegel, D.A., Jannasch, H.W., Johnson, R., Dickey, T. D., McNeil, J., Michaels, A.F., Knap, A.H., 1998. Influence of mesoscale eddies on new production in the Sargasso Sea. Nature 394 (6690), 263–266. https://doi.org/10.1038/28367.

McGillicuddy, D.J., Anderson, L.A., Bates, N.R., Bibby, T., Buesseler, K.O., Carlson, C.A., Davis, C.S., Ewart, C., Falkowski, P.G., Goldthwait, S.A., Hansell, D.A., Jenkins, W.J., Johnson, R., Kosnyrev, V.K., Ledwell, J.R., Li, Q.P., Siegel, D.A., Steinberg, D.K., 2007. Eddy/wind interactions stimulate extraordinary mid-ocean plankton blooms. Science 316 (5827), 1021–1026. https://doi.org/10.1126/science.1136256.

Mobley, C.D., Sundman, L.K., 2013. Hydrolight 5.2 Ecolight 5.2 Technical Documentation. Sequoia Scientific Inc, Bellevue, WA.

Moore, T.S., Matear, R.J., Marra, J., Clementson, L., 2007. Phytoplankton variability off the western Australian coast: mesoscale eddies and their role in cross-shelf exchange. Deep Sea Res. Part II: Topical Stud. Oceanogr. 54 (8–10), 943–960. https://doi.org/10.1016/j.dsr2.2007.02.006.

Nagai, T., Gruber, N., Frenzel, H., Lachkar, Z., McWilliams, J.C., Plattner, G.-K., 2015. Dominant role of eddies and filaments in the offshore transport of carbon and nutrients in the California current system. J. Geophys. Res. Oceans 120 (8), 5318–5341. https://doi.org/10.1002/2015JC010889.

Pickett, M.H., Paduan, J.D., 2003. Ekman transport and pumping in the California current based on the U.S. Navy's high-resolution atmospheric model (COAMPS).J. Geophys. Res. 108 (C10), 3327. https://doi.org/10.1029/2003JC001902.

Pope, R.M., Fry, E.S., 1997. Absorption spectrum (380–700 nm) of pure water. II. Integrating Cavity Measurements. Appl. Opt. 36 (33), 8710–8723. https://doi.org/10.1364/AO.36.008710.

Prieur, L., Sathyendranath, S., 1981. An optical classification of coastal and oceanic waters based on the specific spectral absorption curves of phytoplankton pigments, dissolved organic matter, and other particulate materials. Limnol. Oceanogr. 26 (4), 671–689. https://doi.org/10.4319/lo.1981.26.4.0671.

Roesler, C.S., Perry, M.J., Carder, K.L., 1989. Modeling in situ phytoplankton absorption from total absorption spectra in productive inland marine waters. Limnol. Oceanogr. 34 (8), 1510–1523. https://doi.org/10.4319/lo.1989.34.8.1510.

Romero, O.E., Fischer, G., Karstensen, J., Cermeño, P., 2016. Eddies as trigger for diatom productivity in the open-ocean Northeast Atlantic. Prog. Oceanogr. 147, 38–48. https://doi.org/10.1016/j.pocean.2016.07.011.

Rubio, A., Caballero, A., Orfila, A., Hernández-Carrasco, I., Ferrer, L., González, M., Solabarrieta, L., Mader, J., 2018. Eddy-induced cross-shelf export of high Chl-a coastal waters in the SE Bay of Biscay. Remote Sens. Environ. 205, 290–304. https://doi.org/10.1016/j.rse.2017.10.037.

Sathyendranath, S., Cota, G., Stuart, V., Maass, H., Platt, T., 2001. Remote sensing of phytoplankton pigments: a comparison of empirical and theoretical approaches. Int. J. Remote Sens. 22 (2–3), 249–273. https://doi.org/10.1080/014311601449925.

Seo, H., Miller, A.J., Norris, J.R., 2016. Eddy–wind interaction in the California current system: dynamics and impacts. J. Phys. Oceanogr. 46 (2), 439–459. https://doi.org/10.1175/JPO-D-15-0086.1.

Siegel, D.A., Court, D.B., Menzies, D.W., Peterson, P., Maritorena, S., Nelson, N.B., 2008. Satellite and in situ observations of the bio-optical signatures of two mesoscale eddies in the Sargasso Sea. Deep Sea Res. Part II: Topical Stud. Oceanogr. 55 (10–13), 1218–1230. https://doi.org/10.1016/j.dsr2.2008.01.012.

Siegel, D.A., Peterson, P., McGillicuddy, D.J., Maritorena, S., Nelson, N.B., 2011. Bio-optical footprints created by mesoscale eddies in the Sargasso Sea. Geophys. Res. Lett. 38 (13), 1–6. https://doi.org/10.1029/2011GL047660.

Sun, X., Shen, F., Liu, D., Bellerby, R.G.J., Liu, Y., Tang, R., 2018. In situ and satellite observations of phytoplankton size classes in the entire continental shelf sea, China. J. Geophys. Res.: Oceans 123 (5), 3523–3544. https://doi.org/10.1029/2017JC013651.

Sun, X., Shen, F., Brewin, R.J.W., Li, M., Zhu, Q., 2022. Light absorption spectra of naturally mixed phytoplankton assemblages for retrieval of phytoplankton group composition in coastal oceans. Limnol. Oceanogr. 67 (4), 946–961. https://doi.org/10.1002/lno.12047.

Tang, D., Kawamura, H., Luis, A.J., 2002. Short-term variability of phytoplankton blooms associated with a cold eddy in the northwestern Arabian Sea. Remote Sens. Environ. 81 (1), 82–89. https://doi.org/10.1016/S0034-4257(01)00334-0.

Wang, G., Lee, Z., Mishra, D.R., Ma, R., 2016. Retrieving absorption coefficients of multiple phytoplankton pigments from hyperspectral remote sensing reflectance measured over cyanobacteria bloom waters. Limnol. Oceanogr. Methods 14 (7), 432–447. https://doi.org/10.1002/lom3.10102.

Wang, G., Lee, Z., Mouw, C., 2017. Multi-spectral remote sensing of phytoplankton pigment absorption properties in cyanobacteria bloom waters: a regional example in the western basin of Lake Erie. Remote Sens. (Basel) 9 (12), 1309. https://doi.org/10.3390/rs9121309.

Wang, G., Lee, Z., Mouw, C.B., 2018. Concentrations of multiple phytoplankton pigments in the global oceans obtained from satellite ocean color measurements with MERIS. Appl. Sci. 8 (12), 2678. https://doi.org/10.3390/app8122678.

Wang, Y., Lee, Z., Wei, J., Shang, S., Wang, M., Lai, W., 2021. Extending satellite ocean color remote sensing to the near-blue ultraviolet bands. Remote Sens. Environ. 253, 112228 https://doi.org/10.1016/j.rse.2020.112228.

Zhang, H., Devred, E., Fujiwara, A., Qiu, Z., Liu, X., 2018. Estimation of phytoplankton taxonomic groups in the Arctic Ocean using phytoplankton absorption properties: implication for ocean-color remote sensing. Opt. Express 26 (24), 32280–32301. https://doi.org/10.1364/OE.26.032280.

Zhang, X., Hu, L., He, M.-X., 2009. Scattering by pure seawater: effect of salinity. Opt. Express 17 (7), 5698–5710. https://doi.org/10.1364/OE.26.032280.

Zhang, Z., Wang, W., Qiu, B., 2014. Oceanic mass transport by mesoscale eddies. Science 345 (6194), 322–324. https://doi.org/10.1126/science.1252418.